AN EXPERIMENTAL-NUMERICAL INVESTIGATION OF HEAT TRANSFER DURING SELECTIVE LASER MELTING

M. Masoomi[1], S. M. Thompson[1†], N. Shamsaei[1], A. Elwany[2], L. Bian[3]

[1]Department of Mechanical Engineering, Mississippi State University, Mississippi State, MS 39762
[1]Center for Advanced Vehicular Systems (CAVS), Mississippi State University, Mississippi State, MS 39762
[2]Department of Industrial and Systems Engineering, Texas A & M University, College Station, TX
[3]Department of Industrial and Systems Engineering, Mississippi State University, Mississippi State, MS 39762

[†]Corresponding author:
Email: thompson@me.msstate.edu
Phone: (662) 325 2364

Abstract

The heat transfer in and around a part being fabricated via Selective Laser Melting (SLM) is numerically simulated while considering the surrounding powder bed modeled to have an effective thermal conductivity. By accurately simulating the powder bed heat transfer during SLM, mechanical properties of parts can be better predicted. Heat transfer to previously-deposited layers and the build plate are also simulated. In order to validate the presented model, a thermocouple was embedded into a substrate used and a SLM system was utilized for performing two experiments. In the first set, various laser power and scan speed combinations were employed while passing the laser over the thermocouple-embedded substrate. This procedure calibrated the numerical model and demonstrated that the heat transfer due to convection and radiation during deposition of a single layer is approximately 10-15% of initial laser power input. The final experiment consisted of building a thin wall of SLM of 17-4 PH stainless steel (SS). The effects of scan pattern and part size on the temperature response of and around the part are demonstrated as significant. Distinct heating and cooling rates are also provided for these various cases; indicating the dependency of final microstructure on part size and the utilized scan pattern.

Introduction

Selective Laser Melting (SLM), a Powder Bed Fusion (PBF) additive manufacturing (AM) method, is a unique means for producing complex parts not possible via traditional manufacturing methods. During SLM, a laser beam melts powder material layer by layer to produce a part via solidification. Within an inert atmosphere, a micro-sized melt pool (i.e. molten pool) is induced by a large heat flux via irradiation from a relatively small-diameter laser beam.

The melt pool moves along with the laser beam and solidifies very rapidly upon laser removal, forming a track of solid material. This process is repeated to form multiple tracks with an imposed raster/scan strategy until all individual layers are deposited. After finishing the build, the structure is detached from the substrate, typically via Electrical Discharge Machining (EDM), and then excess powder is removed. SLM methods offer several advantages over traditional 'subtractive' manufacturing methods. Parts with complex geometries can be built more easily and small-lot, customized-application production lines can become more efficient.

Due to the focused laser beam inducing high heat flux via irradiation, SLM parts experience very high, and localized, temperature gradients and heating/cooling rates, resulting in relatively fast melting and solidification. The solidification and cooling rates directly affect and set the microstructure of built parts. Knowledge of the solidifying melt pool behavior upon removal of the laser, including solid phase nucleation and dendritic growth, will indicate the initial microstructure phase and distribution. Secondary solidification, or microstructural evolution, continues at a longer time scale during SLM due to solid phase transformations resulting from cyclic laser-to-substrate conduction. These single and multi-phase heat transfer phenomena are very sensitive to SLM process parameters, such as laser power, laser beam size and traverse speed. In order for SLM parts to function reliably in engineering applications, the relationship between microstructure and final part mechanical properties is paramount [1]. This relationship can be determined either experimentally, numerically or analytically. Since experimental, trial-and-error SLM research can be costly and time-consuming, there is an appeal to use validated numerical simulations for learning process-parameter relationships.

Many have simulated the SLM fabrication of various materials with varying degrees of fidelity in the past several years [2, 3]. Performing numerical simulations allows for time/energy/materials savings by learning process-parameter relationships without repetitious trial-and-error experimentation. In order to numerically simulate powder melting and melt pool solidification during SLM, latent thermal energy transfer needs to be idealized and/or rigorously incorporated into the model. In addition, the simulation of the transient temperature distribution in and around the part during manufacturing needs to be predicted in order to estimate the encumbered part microstructure. The SLM process parameters play a significant role in governing thermal history and thus microstructure type, size and orientation within the part. Via numerical simulation, the sensitivity of thermal history, and thus final microstructure, on various part shapes/sizes and various operating environments (e.g. radiation and convection heat transfer) can be readily performed. In addition, guidelines for effective SLM process control can be ascertained by exploiting any learned relationships between microstructure and heat transfer.

In order to generate trustworthy numerical models, thermal diagnostics of the SLM process is needed in order to benchmark and validate generated numerical data. Espana et al. [4] used thermocouples to measure temperature response during Laser Engineered Net Shaping (LENS). Xiong et al. [5] and Ye et al. [6] used thermocouples and thermography in order to characterize temperature responses during Laser Engineering Net Shaping (LENS). Griffith et al. [7] have reported meaningful temperature responses as provided via thermocouples even after 42 layers of deposition during LENS. In these experiments, the thermocouple bead was exposed atop the substrate and the deposition occurred above and around it. Results of these studies indicate that, due to fast solidification process of the melt pool (which happens in milliseconds), it is hard to monitor its temperature by thermocouples alone. However, knowledge of the

temperature distribution outside the melt pool area allows one to better understand the microstructure evolution and to obtain more data for validating numerical simulations.

Taylor [8] proposed a model to predict the effective thermal conductivity and absorptivity of a sintering surface and benchmarked the model with experimental data obtained via thermocouples exposed to either air or argon atmospheres. Shishkovsky [9] measured the temperature response around the melting area during the Selective Laser Sintering (SLS) of metal-polymer, intermetallic and ceramic materials using five thermocouples (temperature range 400-2800 ºC). In addition to these experimental approaches, there exist analytical and numerical methods for estimating the temperature response during SLM. For instance, it is common to employ Rosenthal's classical analytical solution to determine temperature distribution in media with a moving heat source problem [10]. Numerical methods, such as the Finite Element (FE) and Finite Difference (FD) methods, are used to solve more complex problems. Dong et al. [11] used the FE method to study the effects of phase transformation as well as to determine the influence of scanning speed, laser intensity and beam spot diameter on SLS parts during manufacture. Riedlbauer et al. [3] investigated the SLM melt pool temperature profile and its size by using a nonlinear FE method.

There are different methods for varying local cooling rates during the SLM process, including the variation of process parameters such as laser power, laser speed, hatching space and thickness of each layer. Variation of these parameters would impact the melt pool temperature and consequently alter cooling rates. However, it is possible that, upon changing process parameters during SLM, the porosity of the part can increase due to lack of fusion and/or melt pool instability. Hence, to ensure ideal deposition and solidification conditions, parameter sets, not individual parameters, should vary with time to ensure full-density and target microstructure. The combination of process parameters for ensuring near- or fully-dense parts depends on the utilized material, powder size and the building time.

Since real-time process control of SLM is not fully available within the state-of-the-art, it is of interest to work with time-invariant process parameters during SLM. For constant process parameters, one can, for example, employ unique scan patterns to overcome effects of part size and geometry. Hence, in this study, effects of scan pattern on cooling rates during SLM will be studied. Also the effectiveness of changing them will be compared to changing the process parameters.

Analysis

This case study focused on the fabrication of 17-4 precipitation hardened (PH) stainless steel (SS). Numerical simulations were performed by first discretizing both space and time in order to solve the partial-differential, conservation equations for energy. The temperature through the solidified part and powder bed was assumed to be governed by a non-homogeneous heat equation with Fourier-type conduction. The heat equation governing temperature along a single layer can be written as:

$$\rho(t)c(t)\frac{\partial T(x,y,z,t)}{\partial \mathrm{t}} = k(t)\nabla^2 T(x,y,z,t) + Q(x,y,t) \quad (1)$$

where $\rho(t)$ is temperature-dependent density of SS 17-4 PH, $c(t)$ is the temperature-dependent specific heat capacity of SS 17-4 PH, $k(t)$ is temperature-dependent thermal conductivity of SS 17-4 PH [12], T is temperature and Q is a volumetric heat source term assumed to be the irradiation flux density at the melt pool interface, i.e.:

$$Q = \alpha G = f(r) \tag{2}$$

where α is the absorptivity (assumed constant) of the material and G is the laser power at a given location. The laser power with Gaussian form is formulated as:

$$G \cong \frac{2P}{\pi R^2} \exp\left(-\frac{2r^2}{R^2}\right) \tag{3}$$

where P is laser power, R denotes the effective laser beam radius at which the energy density reduces to $1/e^2$ at the center of the laser spot, r is the radial distance from the center of the laser spot [2]. The latent heat transfer associated with powder melting and melt pool solidification was modeled using:

$$q = mL \tag{4}$$

where q is the energy released or absorbed during the change of phase, m is the mass of substance and L is the specific latent heat of fusion for a particular substance. The boundary conditions considered both convection and thermal radiation based on the exposed surface of the current layer to the surroundings, i.e.:

$$q_{\mathrm{c}} = h(T - T_{0\mathrm{c}}) \tag{5}$$

$$q_{\mathrm{r}} = \sigma\varepsilon\left(T^4 - {T_{0\mathrm{r}}}^4\right) \tag{6}$$

where h is the heat transfer coefficient, σ is the Stefan-Boltzmann constant and ε is the emissivity. Also, $T_{0\mathrm{c}}$ represents the temperature of gas inside the chamber and $\mathrm{T}_{0\mathrm{r}}$ represents the chamber surroundings temperature. The heat transfer coefficient was assumed as uniform and was calculated based on the velocity and the type of gas inside chamber. Given the small size of the melt pool relative to the SLM chamber, gray body/enclosure-type radiation behavior exists and Eq. (6) holds. The absorbed energy from the heat source it utilized for melting the powder or transfers through the powder bed, at a rate of q_{cond}, or dissipates to the surroundings, i.e.:

$$Q = q + q_{\mathrm{c}} + q_{\mathrm{r}} + q_{\mathrm{cond}} \tag{7}$$

By solving Eq. 1, the temperature profile along a layer can be obtained in all points at all time. While adding a new layer, a previously-deposited layer has time to cool via powder-bed heat transfer or to the surrounding environment.

Numerical Simulation

Numerical simulations were performed using the commercially-available COMSOL 4.4 Multiphysics FE software. The powder bed was assumed to be a homogenous and continuous medium and the laser heat source possesses a Gaussian intensity distribution (Eq. 3). The effective thermal conductivity of the powder bed was calculated using:

$$k_{\mathrm{pb}} = k_{\mathrm{s}}(1 - \phi) \tag{7}$$

where k_{pb} and k_{s} are the thermal conductivity of powder bed and solid powder, respectively. Porosity of powder bed, ϕ can be written as:

$$\phi = \frac{\rho_{\mathrm{s}} - \rho_{\mathrm{p}}}{\rho_{\mathrm{s}}} \tag{8}$$

where ρ_{s} and ρ_{s} are densities of solid material and powder bed, respectively. For the current investigation, the porosity of the powder bed was 60%. A time step of Δt = 0.1 s was utilized for the current investigation, so it could capture all the transient responses. Free triangular elements were chosen for the meshing scheme. In order to better model the high heat flux transport near the laser/liquid interface, the element size in this region was selected as $L \sim 20$ μm. Element sizes increased with distance from the high heat flux zone to a size of L = 100 μm, as shown in Fig. 1. The heat transfer coefficient was estimated based on the gas inside the chamber, its velocity and the geometry of the problem. Based on Reynolds number (3.04×10^4), Prandtl number (0.68) and Nusselt number (102), the heat transfer coefficient is 12.7 W/m²·K. Finally, the initial condition for the powder and 17-4 stainless steel substrate was set as 20 ºC. Mesh independent results were obtained by reducing the size of the mesh to the size that results were not affected by the size of mesh. Parallel supercomputing resources were utilized to simulate the manufacturing process.

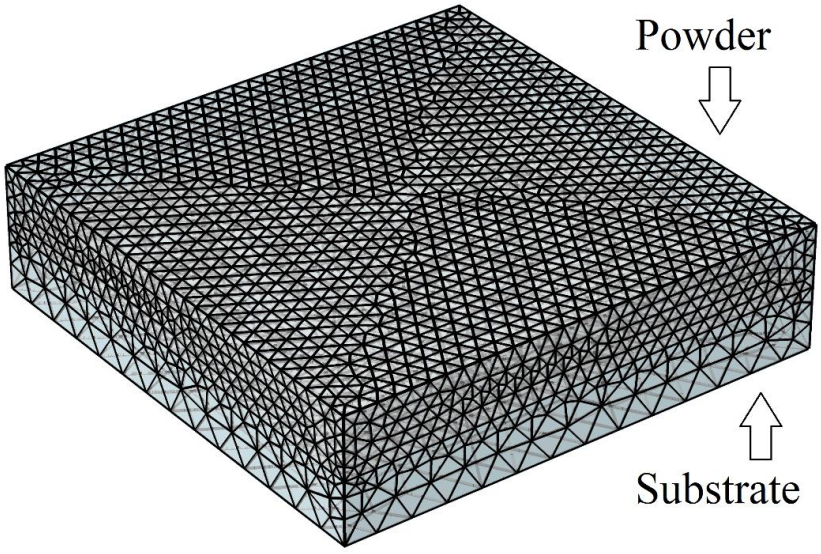

Figure 1. Meshing scheme used for simulations showing one layer of powder and substrate

Experimental Setup and Procedure

Experiments were conducted using a PHENIX PM 100 SLM system. The particular SLM system uses a fiber laser (Photonics) with Gaussian profile intensity, 50 W power limit, 1075 nm wavelength and spot size of 70 μm. All experiments were performed under argon atmosphere, pumped into the 200 L chamber at a rate of 167 cm^3/s. Substrate temperature was monitored using, an embedded, pre-calibrated Type-C thermocouple (OMEGA, bead diameter ≅ 0.075 mm) as shown in Fig. 2. Temperature data were recorded using an ICP DAS I-7018 data logger

at a rate of 1 Hz. For the typical temperature range recorded, the maximum error associated with the thermocouples was 4.5 ˚C (±1%), while nominal error of the data logger was 0.2 %.

The material used in the process was SS 17-4 PH powder. The average particle size was 25 μm with a room-temperature thermal conductivity of approximately 12 W/m·K. The absorption coefficient, α, was assumed to be constant at 0.3 as suggested by [13, 14]. Two different sets of experiment were performed. The first experiment was performed without powder in the machine. The laser moved from the starting point, as shown in Fig. 2, to the edge of the plate a single time. During this experiment, three different laser speeds and powers were employed and these parameters are summarized in Table 1. The scan pattern was only performed once and then the substrate was allowed to cool back to room-temperature before a new set was performed.

Table 1. Process parameters utilized for nine laser scans along thermocouple-embedded substrate

Power\speed	50 mm/s	150 mm/s	250 mm/s
25.0 W	Exp. #1	Exp. #2	Exp. #3
37.5 W	Exp. #4	Exp. #5	Exp. #6
50.0 W	Exp. #7	Exp. #8	Exp. #9

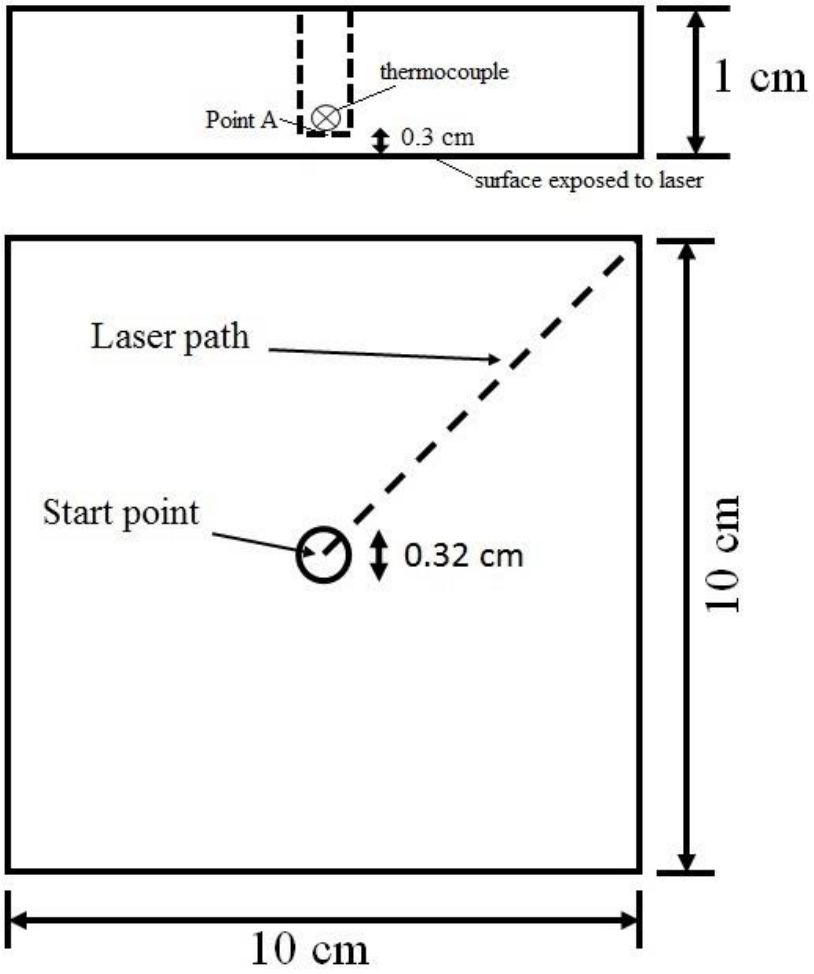

Figure 2. Dimensions of thermocouple-embedded substrate with start point and laser path [15]

The second experiment was designed for fabricating a thin wall structure atop the thermocouple-embedded substrate. The length and width of the wall was 50 mm and 2 mm, respectively. The thin wall was constructed using a laser scan pattern shown in Fig. 2. The process parameters were held constant with time and consisted of a 50 W laser power and 50 mm/s scan speed. All of the results from experiment were used to verify the numerical simulations. The substrate design and powder bed were ensured to match those related to the SLM machine/process utilized for validation experiments.

Results and Discussion

The temperature response at Point A (shown in Fig. 2), as measured experimentally and numerically for Exp. #7 (single laser pass) is shown in Fig. 3. For the numerical simulation of this experiment, the temperature under the substrate (Point A) was extracted after simulating heat transfer through powder and substrate. The results demonstrate that the temperature within the substrate during laser exposure does not surpass 60 ºC, and that the substrate cools within ~ 15 s. However, the experimental data appears to agree well with numerical data for all experiments conducted, i.e. Exps. #1 - #9. The numerical model approach is shown to be validated in Fig. 3.

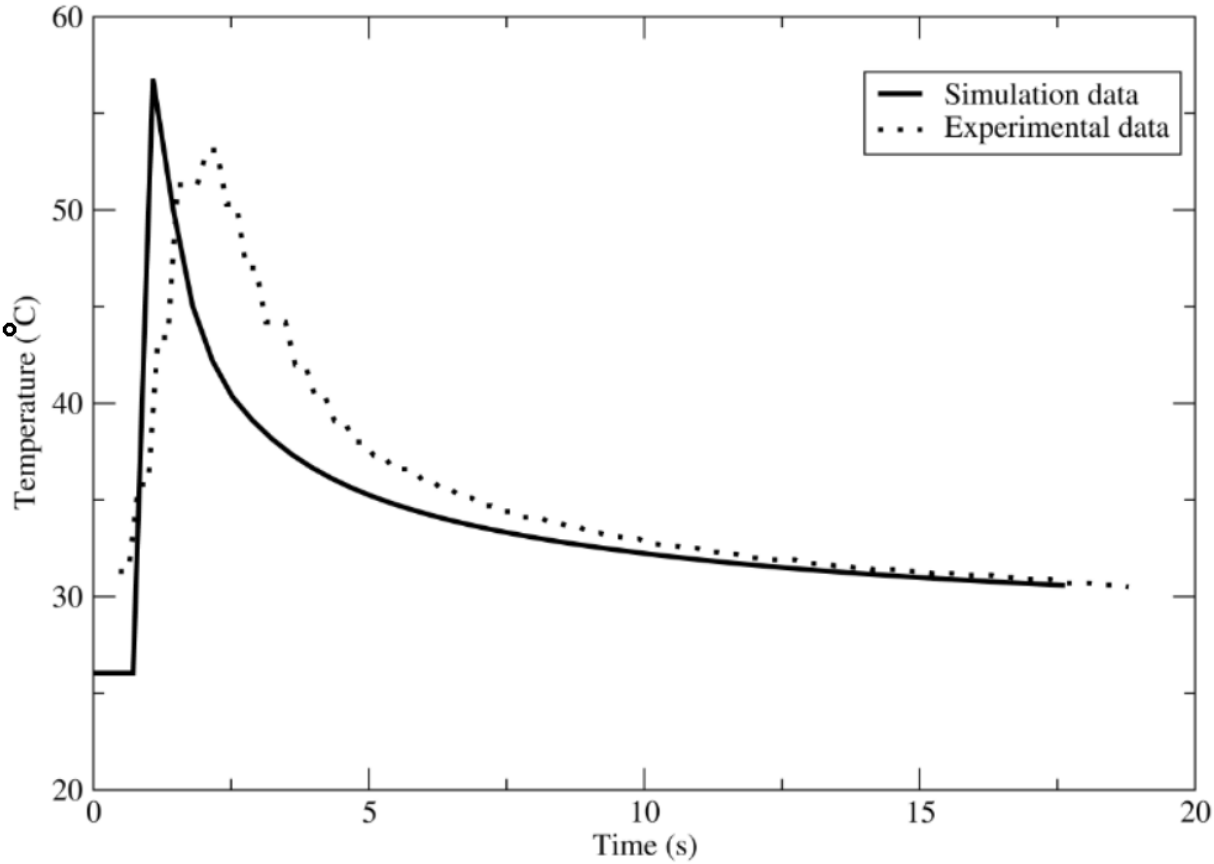

Figure 3. Variation of temperature at Point A with respect to time during Exp. 7 laser scanning.

Figure 4 shows the simulated substrate temperature response during deposition of the SS 17-4 PH thin wall while using the same parameters from Exp. #7. The first layer of the thin wall is presented, and the multi-track scan pattern shown in Fig. 2 is utilized. The effect of scan pattern on the temperature response at Point A below the substrate is clearly evidenced by the multiple temperature peaks vs. time. Note that the experimental data is not oscillatory due to the employed temperature collection frequency; however, the general temperature rise agrees very well with the numerical simulation. During deposition of one layer, the temperature of the substrate has increased by 25 ºC, to a maximum temperature near 50 ºC. Note that the temperature cycling amplitude appears to reduce as the laser gets closer and closer to Point A.

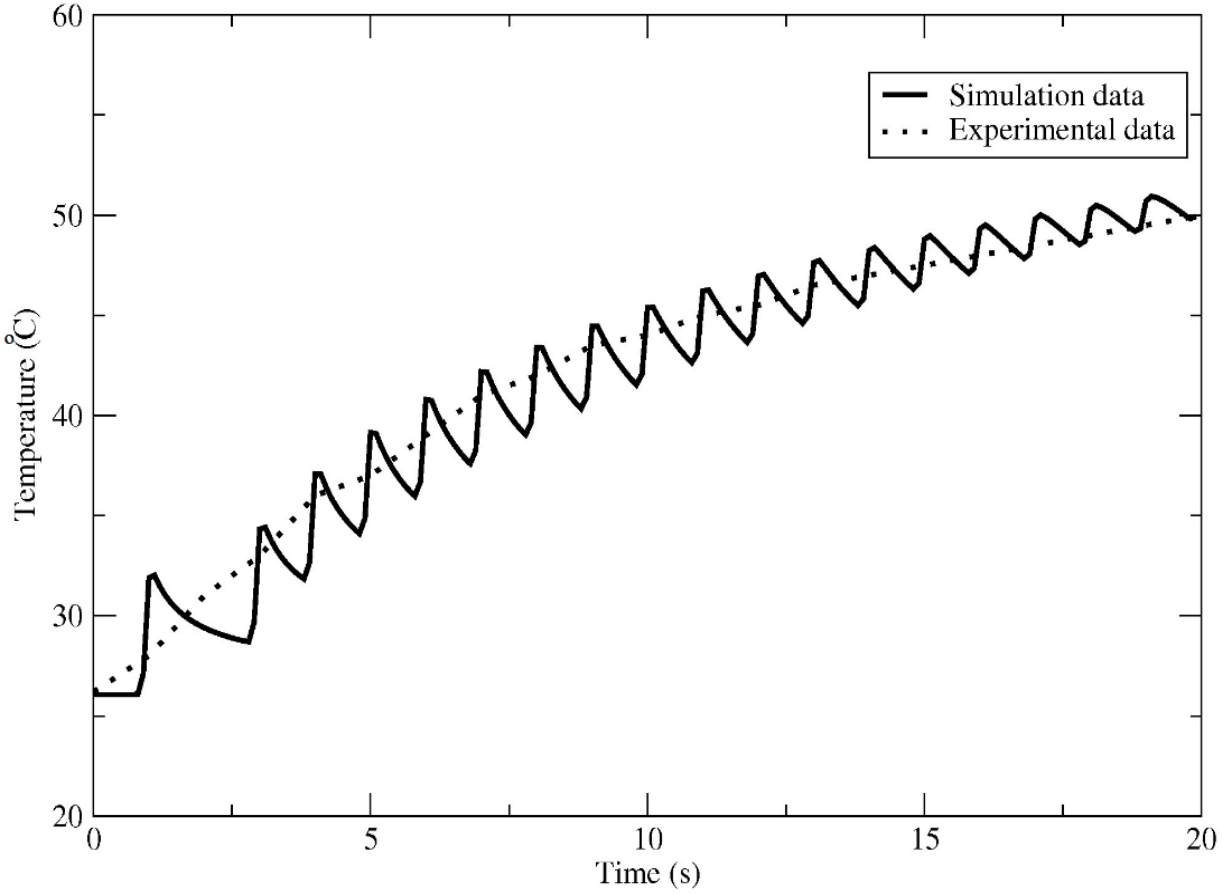

Figure 4. Variation of temperature at Point A with respect to time during SS 17-4 PH thin wall build using Exp. #7 process parameters and scan pattern.

The effects of laser scan pattern on the temperature response was investigated by using each of the three scan patterns shown in Fig. 5 for the simulated SLM fabrication of a SS 17-4 PH thin wall. From Fig. 5, it may be seen that the laser can pass parallel to any edge of the wall, go back-and-forth or just in one direction parallel with the wall length.

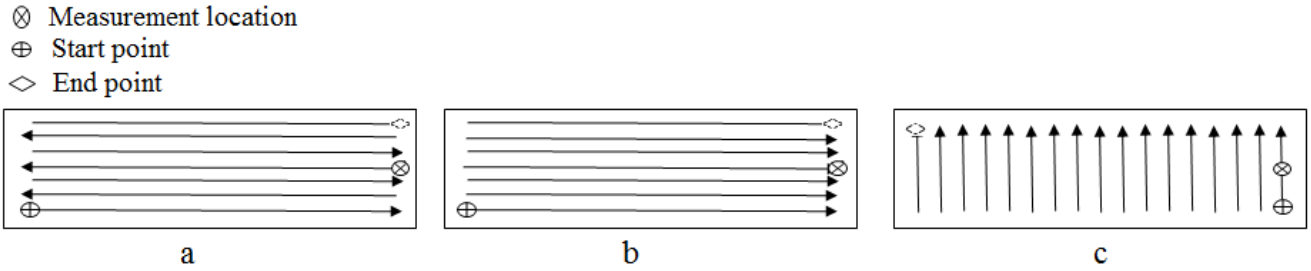

Figure 5. Scan patterns investigated: (a) alternating, (b) unidirectional/lengthwise and (c) unidirectional/widthwise

The temperature response of Point A for all three scan patterns, using process parameters from Exp. #7, is shown in Fig. 6. From Fig. 6, it may be seen that each laser scan pattern provides for a unique temperature response at Point A within the substrate, and thus, a different temperature response in the surrounding powder bed and part. The results show that, like the trend observed in Fig. 4, the temperature oscillations decrease in amplitude as the laser approaches the measurement point. Hence, the severity of temperature fluctuations is decreased as the bulk part temperature increases for a given layer. The alternating, zig-zag pattern (e.g. scan pattern #a) provided for the hottest peak temperatures and largest temperature amplitudes. Note that although the time invested per layer for all of three scan patterns is the same, the deposited part will experience completely different cooling and heating rates – as evidenced by the amplitude and frequency of the temperature oscillations at Point A. These different cooling rates will directly impact the encumbered part microstructure, and thus provides a means to control part thermal history without changing process parameters in real-time.

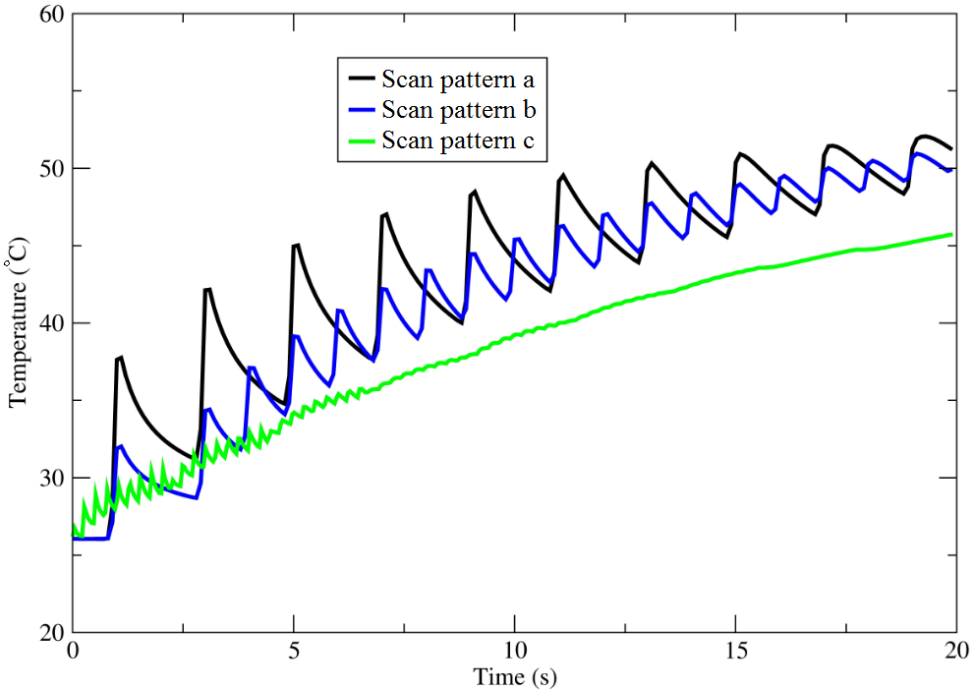

Figure 6. Variation of temperature at measurement location (Point A) with respect to time during SS 17-4 PH thin wall build using Exp. #7 process parameters and three different scan patterns

The heating and cooling rates (i.e. temperature time rate of change) while laser moving in one direction or moves back and forth presented in Fig. 7 and Fig. 8. The temperature was obtained through the simulation of thin wall build. Process parameters are same as Exp. #7. By comparing Fig. 7 and Fig. 8, it is obvious that temperature rate is strongly dependent on scan pattern. Scan pattern (b) nearly double the peak rate. By knowing the effects of scan pattern on thermal response, controlling the temperature rate become feasible.

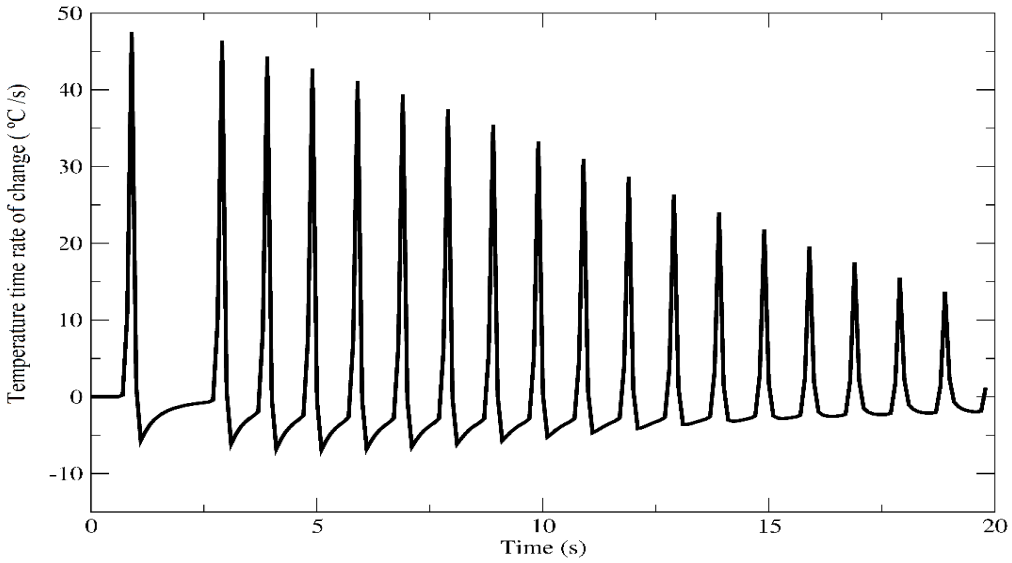

Figure 7. Temperature time rate of change at measurement location with respect to time using Exp. #7 process parameters with scan pattern (b)

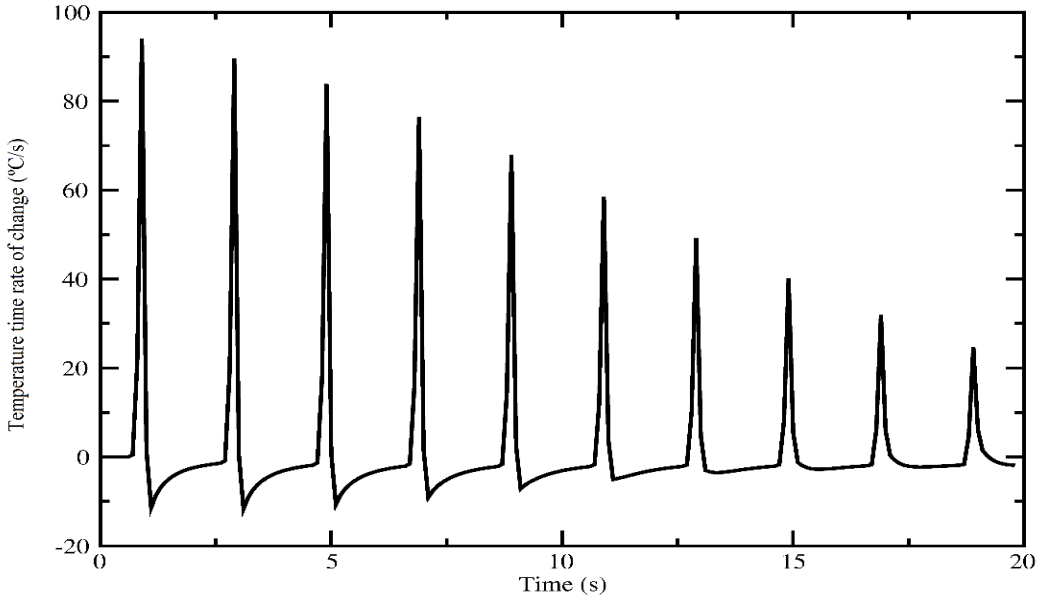

Figure 8. Temperature time rate of change at measurement location with respect to time using Exp. #7 process parameters with scan pattern (a)

The effects of geometry on temperature response and cooling rate were studied by fabricating a thin wall with various lengths via simulation. As shown in Fig. 9, a 2 mm thick wall with a length of 20 mm, 30 mm or 40 mm was constructed. The 'alternating' scan pattern, Fig. 5 a, and process parameters from Exp. #7 were utilized. The results for the first deposited layer are provided in Figs. 10-11.

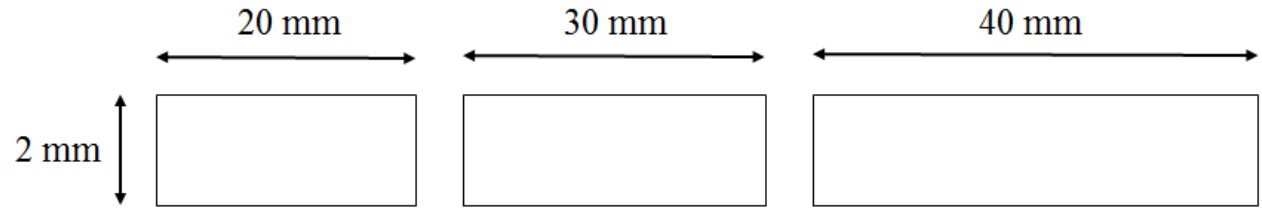

Figure 9. Thin wall dimensions

In Figure 10, it is obvious that as the length of the thin wall decreases, for a given set of process parameters and scan pattern, the peak temperature increases. For length of sample reduce from 40 mm to 20 mm, the peak temperature increase from 50 ˚C to 57 ˚C. the time of the build will decrease as the size decrease too, so we expect that heating rate would increase as length of part decrease.

The heating/cooling rates are also influenced by the geometry of the part, as shown in Fig. 11. It may be seen that the cooling rate increases as the length of the wall decreases. However, the opposite is true for heating rate. The wall with length of 30 mm has the highest heating rate while heating rate of the other two walls is nearly the same.

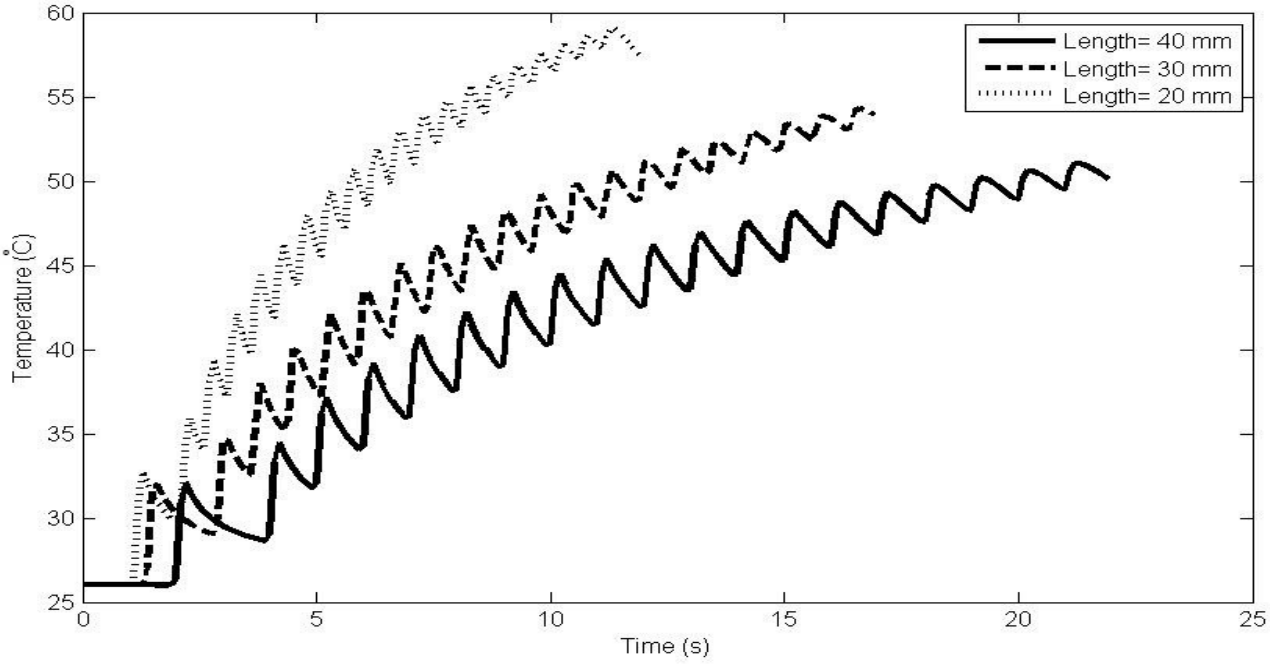

Figure 10. Variation of temperature at measurement location with respect to time using Exp. #7 process parameters with three different geometries

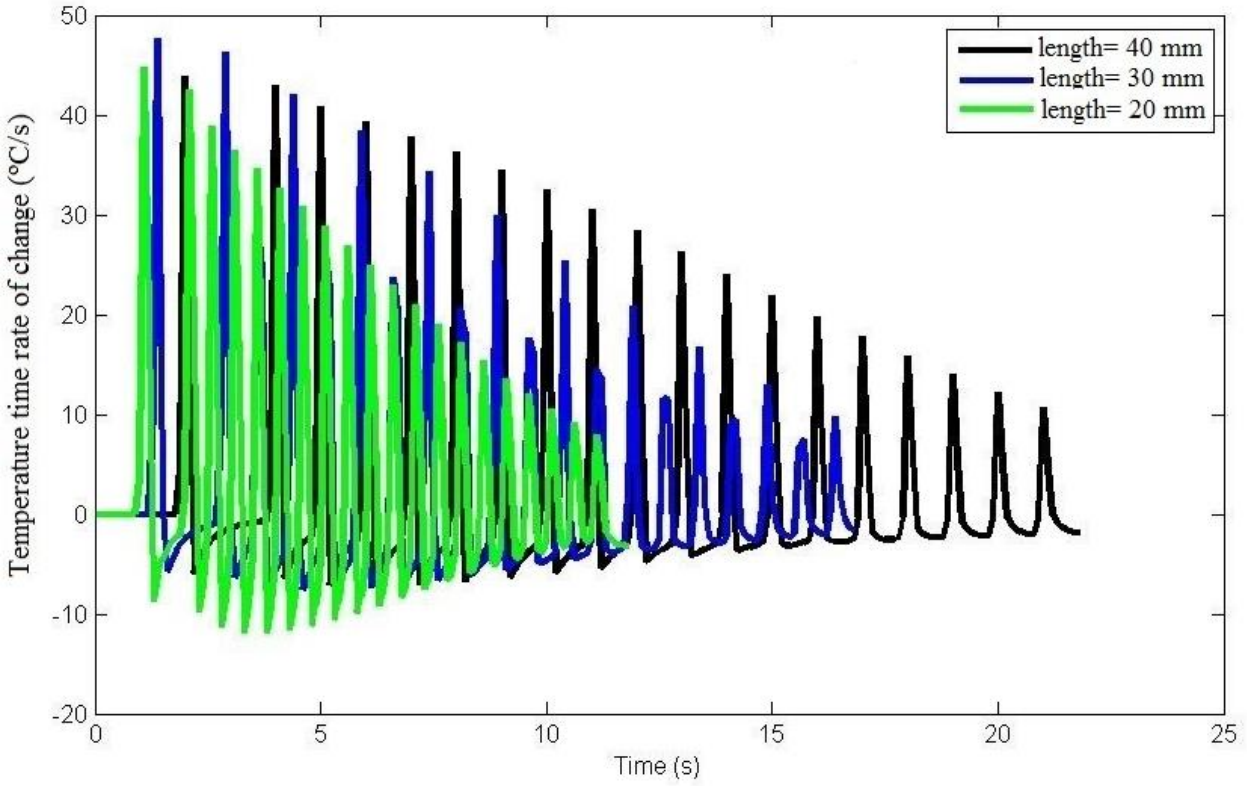

Figure 11. Temperature time rate of change at measurement location with respect to time using Exp. #7 process parameters with three different geometries

Conclusions

The purpose of this research was to provide the tools to predict the heat transfer through the parts, powder and substrate. The feedback from model and thermocouples measurements could be used to decide whether the remaining portion of the powder is recyclable or not. Also results, temperature distribution, cooling and heating rate, are necessary for determining the microstructure formation. Finally effects of process parameters and built patterns on heat transfer were studied The model used to predict the temperature and rate of change of it over time for different geometry and scan pattern. It has shown that by changing these parameters, parts experience different thermal history. These results could be used to design the built pattern based on the geometry to get uniform response even with different geometry.

It is understood from these simulations that by changing process parameters, scan pattern and geometry, completely different peak temperature can be obtained. Also each point in the part experiences different cooling rate. So the final product of SLM machine is non homogenous part which its mechanical properties is dependent on the process parameters, built pattern and the geometry. In order to solve the problem, the parts can be heat treated using classical methods. Also by designing unique built pattern based on geometry and adopting suitable process parameters more homogenous parts with same mechanical properties can be built

To summarize, results could be divided into four groups, temperature distribution, heat transfer, cooling and heating rate. Numerical modeling is capable to give information of entire thermal behavior. All un-melted powder remaining in the SLM machine is sought to be recycled for later use without detriment. However, un-melted powder near the part will undergo a degree of thermal cycling and may impact its recyclability.

Acknowledgements

This work was financially supported by Mississippi State University's Office of Research and Economic Development (ORED) and Center for Advanced Vehicular Systems (CAVS). Authors acknowledge the resources provided by Mississippi State University's High Performance Computing Collaboratory (HPC²).

References

[1] L. Bian, S. M. Thompson and N. Shamsaei, "Mechanical Properties and Microstructural Features of Direct Laser Deposited Ti-6Al-4V," *JOM TMS,* vol. 67, no. 3, pp. 629-638, 2014.

[2] Y. Li and D. Gu, "Parametric analysis of thermal behavior during selective laser melting additive manufacturing of aluminum alloy powder," *Materials and Design,* vol. 63, pp. 856-867, 2014.

[3] D. Riedlbauer, "Modelling, simulation and experimental validation of heat transfer in selective laser melting of the polymeric material PA12," *Computational Materials Science,* vol. 93, pp. 239-248, 2014.

[4] F. A. España, V. K. Balla and A. Bandyopadhyay, "Laser surface modification of AISI 410 stainless steel with brass for enhanced thermal properties," *Surface & Coatings Technology,* vol. 204, p. 2510–2517, 2010.

[5] Y. Xiong, W. Hofmeister, Z. Cheng, J. Smugeresky, E. Lavernia and J. Schoenung, "In situ thermal imaging and three-dimensional finite element modeling of tungsten carbide–cobalt during laser deposition," *Acta Materialia,* vol. 57, p. 5419–5429, 2009.

[6] R. Ye, "Numerical modeling of the thermal behavior during the LENS® process," *Materials Science and Engineering,* vol. 428, pp. 47-53, 2006.

[7] M. L. Griffith , M. E. Schlienger , L. D. Harwell , M. S. Oliver , M. D. Baldwin , M. T. Ensz , M. Essien , J. Brooks , C. V. Robino , J. E. Smugeresky , W. H. Hofmeister , M. J. Wert and D. V. Nelson , "Understanding thermal behavior in the LENS process," *Materials & Design,* vol. 20, pp. 107-113, 1999.

[8] C. Taylor, Direct laser sintering of stainless steel : thermal experiments and numerical modelling, University of Leeds, 2004.

[9] I. V. Shishkovsky, "Surface Laser Sintering of exothermic powder compositions," *Journal of Thermal Analysis and Calorimetry,* vol. 91, pp. 427-436, 2008.

[10] D. Rosenthal and R. H. Carmern, "Temperature distribution in cylinder heated by point source moving along its axis," *Trans. A.S.M.E.,* vol. 69, pp. 961-968, 1947.

[11] L. Dong, "Three-dimensional transient finite element analysis of the selective laser sintering process," *Journal of Materials Processing Technology,* vol. 209, no. 2, pp. 700-706, 2009.

[12] R. W. Powell, C. Y. Ho and P. E. Liley, Thermal conductivity of selected materials, National bureau of standards, 1966.

[13] B. Valsecchi, B. Previtali, E. Gariboldi and A. Liu, "Characterisation of the Thermal Damage in a Martensitic Steel Substrate Consequent to Laser Cladding Process," *Procedia Engineering,* vol. 10, p. 2851–2856, 2011.

[14] C. M. Taylor and T. H. C. Childs, "Thermal experiments in direct metal laser sintering," in *Proceedings of 9 Assises Européennes du Prototypage Rapide and 10 European Conference on Rapid Prototyping and Manufacturing (EURO RP 2001)*, Paris, 2001.

[15] M. Masoomi, E. Alaa, N. Shamsaei and S. Thompson, "Modeling, simulation and experimental validation of heat transfer during selective laser melting," in *Proceedings of the ASME 2015 International Mechanical Engineering Congress & Exposition*, Houston, 2015.